



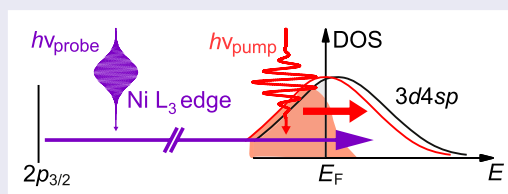
# The interplay of local electron correlations and ultrafast spin dynamics in fcc Ni

Tobias Lojewski<sup>a</sup>, Mohamed F. Elhanoty<sup>b</sup>, Loïc Le Guyader<sup>c</sup>, Oscar Grånäs<sup>b</sup>, Naman Agarwal<sup>c†</sup>, Christine Boeglin<sup>d</sup>, Robert Carley<sup>c</sup>, Andrea Castoldi<sup>e,f</sup>, Christian David<sup>g</sup>, Carsten Deiter<sup>c</sup>, Florian Döring<sup>g</sup>, RobinY Engel<sup>h</sup>, Florian Erdinger<sup>i,‡</sup>, Hans Fangohr<sup>c,j,k</sup>, Carlo Fiorini<sup>e,f</sup>, Peter Fischer<sup>i</sup>, Natalia Gerasimova<sup>c</sup>, Rafael Gort<sup>c</sup>, Frank deGroot<sup>l</sup>, Karsten Hansen<sup>h</sup>, Steffen Hauf<sup>c</sup>, David Hickin<sup>c</sup>, Manuel Izquierdo<sup>c</sup>, Benjamin E. Van Kuiken<sup>c</sup>, Yaroslav Kvashnin<sup>b</sup>, Charles-Henri Lambert<sup>m</sup>, David Lomidze<sup>c</sup>, Stefano Maffessanti<sup>h</sup>, Laurent Mercadier<sup>c</sup>, Giuseppe Mercurio<sup>c</sup>, Piter S. Miedema<sup>h</sup>, Katharina Ollefs<sup>a</sup>, Matthias Pace<sup>d</sup>, Matteo Porro<sup>c,n</sup>, Javad Rezvani<sup>o</sup>, Benedikt Rösner<sup>g</sup>, Nico Rothenbach<sup>a</sup>, Andrey Samartsev<sup>c,h</sup>, Andreas Scherz<sup>c</sup>, Justina Schlappa<sup>c</sup>, Christian Stamm<sup>m,p</sup>, Martin Teichmann<sup>c</sup>, Patrik Thunström<sup>b</sup>, Monica Turcato<sup>c</sup>, Alexander Yaroslavltssev<sup>b,c</sup>, Jun Zhu<sup>c</sup>, Martin Beye<sup>h</sup>, Heiko Wende<sup>a</sup>, Uwe Bovensiepen<sup>a</sup>, Olle Eriksson<sup>b</sup> and Andrea Eschenlohr<sup>a</sup>

<sup>a</sup>Faculty of Physics and Center for Nanointegration Duisburg-Essen (CENIDE), University of Duisburg-Essen, Duisburg, Germany; <sup>b</sup>Department of Physics and Astronomy, Uppsala University, Uppsala, Sweden; <sup>c</sup>European XFEL, Schenefeld, Germany; <sup>d</sup>CNRS, Institut de Physique et Chimie des Matériaux de Strasbourg, Université de Strasbourg, Strasbourg, France; <sup>e</sup>Dipartimento di Elettronica, Informazione e Bioingegneria Politecnico di Milano, Milano, Italy; <sup>f</sup>Istituto Nazionale di Fisica Nucleare, Sez. Milano, Milano, Italy; <sup>g</sup>Paul Scherrer Institut, Villigen PSI, Switzerland; <sup>h</sup>Deutsches Elektronen-Synchrotron DESY, Hamburg, Germany; <sup>i</sup>Institute for Computer Engineering, University of Heidelberg, Heidelberg, Germany; <sup>j</sup>Max-Planck Institute for the Structure and Dynamics of Matter, Hamburg, Germany; <sup>k</sup>University of Southampton, Southampton, UK; <sup>l</sup>Materials Chemistry and Catalysis (MCC), Debye Institute for Nanomaterials Science Utrecht University, Utrecht, Netherlands; <sup>m</sup>Department of Materials, ETH Zurich, Zurich, Switzerland; <sup>n</sup>Department of Molecular Sciences and Nanosystems, Ca' Foscari University of Venice, Venezia, Italy; <sup>o</sup>Laboratori Nazionali di Frascati, INFN, Frascati (Roma), Italy; <sup>p</sup>Institute for Electric Power Systems, University of Applied Sciences and Arts Northwestern Switzerland, Windisch, Switzerland

## ABSTRACT

The complex electronic structure of metallic ferromagnets is determined by a balance between exchange interaction, electron hopping leading to band formation, and local Coulomb repulsion. By combining high energy and temporal resolution in femtosecond time-resolved X-ray absorption spectroscopy with *ab initio* time-dependent density functional theory we analyze the electronic structure in fcc Ni on the time scale of these interactions in a pump-probe experiment. We distinguish transient broadening and energy shifts in the absorption spectra, which we demonstrate to be captured by electron repopulation respectively correlation-induced modifications of the electronic structure, requiring to take the local Coulomb interaction into account.



## IMPACT STATEMENT

We demonstrate that local correlations are essential for the transient electronic structure of optically excited Ni; paving the way for analyzing these interactions on their intrinsic timescales in correlated materials.

## ARTICLE HISTORY

Received 23 March 2023

## KEYWORDS

Ferromagnetism; local correlations; ultrafast dynamics; time-resolved x-ray absorption spectroscopy; time-dependent density functional theory

**CONTACT** Andrea Eschenlohr ✉ [andrea.eschenlohr@uni-due.de](mailto:andrea.eschenlohr@uni-due.de) Faculty of Physics and Center for Nanointegration Duisburg-Essen (CENIDE), University of Duisburg-Essen, Lotharstr.1, Duisburg 47057, Germany

<sup>†</sup>Present address: Department of Physics and Astronomy (IFA), Aarhus University, NY Munkegade 120, 8000 Aarhus C, Denmark

<sup>‡</sup>Present address: EXTOLL GmbH, 68159 Mannheim, Germany

Supplemental data for this article can be accessed here. <https://doi.org/10.1080/21663831.2023.2210606>

© 2023 The Author(s). Published by Informa UK Limited, trading as Taylor & Francis Group.

This is an Open Access article distributed under the terms of the Creative Commons Attribution-NonCommercial License (<http://creativecommons.org/licenses/by-nc/4.0/>), which permits unrestricted non-commercial use, distribution, and reproduction in any medium, provided the original work is properly cited. The terms on which this article has been published allow the posting of the Accepted Manuscript in a repository by the author(s) or with their consent.

Magnetic order in the 3d transition metals Fe, Co, Ni and their alloys arises from the effects of exchange interaction, local correlations, and the electronic band structure (electronic hopping) [1]. Solid state spectroscopy in conjunction with advanced electronic structure calculations [2] resolves the underlying microscopic processes in the thermodynamic ground state [3] as well as electron, spin, and lattice excitations [4,5]. For fcc Ni, the imaginary part of the self-energy representing the scattering rate  $\Gamma$  increases from the Fermi energy ( $E_F$ ) up to 2 eV above from 100 meV to 500 meV [2] or, following  $\tau = \hbar/\Gamma$ , the scattering time  $\tau$  decreases from 6 to 1 fs. Time domain methods probe these ultrafast timescales directly and have revealed the optically induced ultrafast demagnetization of the 3d ferromagnets, i.e. the transient reduction of the magnetic moment due to fs laser pulses mediated by spin-orbit interaction on  $\approx 100$  fs and by spin wave excitations on several ps time scales [6,7]. The underlying processes are based on spin-orbit mediated spin flips [8–10], spin transfer [11–13], spin-lattice coupling, and the principle of angular momentum conservation [14,15]. However, a comprehensive picture of the transient electronic structure is still lacking because the competition (or cooperation) of magnetic order, local correlations, and the optical excitation in a regime beyond a weak perturbation cannot yet fully be accounted for.

Here, we establish the influence of local electronic Coulomb interactions on the spin-dependent electron dynamics in fcc Ni in the time domain. This finding is based on exploiting high energy resolution in fs time-resolved X-ray absorption spectroscopy (tr-XAS) experiments at the Ni  $L_{2,3}$  absorption edges which we analyze quantitatively with *ab initio* time-dependent density functional theory (TDDFT) including local electron correlations.

Figure 1(a) sketches the pump-probe experiment which measures the temporal correlation of ultrashort X-ray probe pulses tuned to the Ni  $L_{2,3}$  edges with near-infrared pump pulses of photon energy  $h\nu = 1.5$  eV, 35 fs duration, and  $12 \text{ mJ/cm}^2$  incident fluence as a function of time delay  $\Delta t$ . The core level resonance involves a transition from  $2p_{3/2}$  ( $2p_{1/2}$ ) to  $3d4sp$  final states at the  $L_3$  ( $L_2$ ) absorption edge. Thereby, we analyze the effect of the optical excitation on the unoccupied  $3d4sp$  electronic density of states (DOS) through the time-dependent absorption changes.

The experiments were performed at the Spectroscopy and Coherent Scattering Instrument (SCS) of European XFEL [16,17]. Spectra of 20 nm fcc Ni layers [18] were measured using linearly polarized monochromatic X-ray pulses with  $\Delta E/E = 5 \cdot 10^{-4}$  [19] tuned between 840 and 880 eV to cover the  $L_2$  and  $L_3$  absorption edges [20]. The

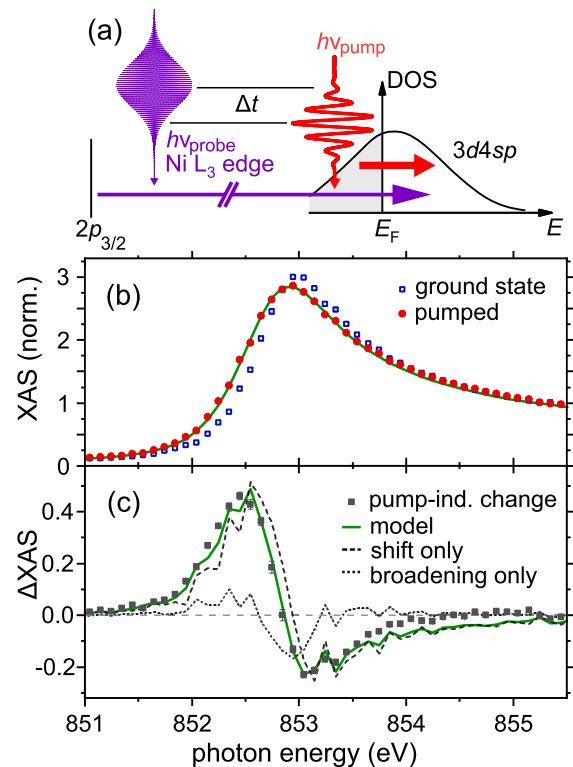


**Figure 1.** (a) Near-infrared pump, soft x-ray absorption probe experiment at the Ni  $L_3$  absorption  $2p_{3/2} \rightarrow 3d4s$  analyzing the transiently modified electronic density of states above  $E_F$  at time delay  $\Delta t$ . (b) Ground state (blue squares) and pumped (circles) absorption spectrum at  $\Delta t = 0.4$  ps. The pump-induced changes  $\Delta XAS$  are modeled (green line) based on the static absorption spectrum which allows to distinguish the contributions of an energy shift and broadening. (c) Pump-induced change (black squares) including the modeling result in (b) (green line). The dashed (dotted) line indicates fits to the measured  $\Delta XAS$  with only an energy shift (broadening), which are insufficient to describe the data.

employed X-ray delivery time pattern consisted of fifty 50 fs X-ray pulses in one train with a train repetition rate of 10 Hz and an intra-train repetition rate of 70 kHz. The pump pulses [16,21] were synchronized with every second X-ray pulse. A transmission zone plate [22,23] splits the incoming X-rays into three focused, spatially distinct beams of equal intensity in diffraction orders  $-1$ ,  $0$ ,  $1$ . This setup allowed the simultaneous detection of the pumped, unpumped, and a reference signal for the identical X-ray pulse, which is essential at a SASE-free electron laser due to fluctuations in the intensities of subsequent pulses and was made possible by a MiniSDD-based DSSC detector, a 1Mpixel camera with a peak frame rate up to 4.5 MHz [24]. The time resolution of the experiment was 80 fs full width at half maximum (FWHM). XAS was recorded at room temperature in transmission geometry and evaluated using a dedicated toolbox [16,25–28]. The

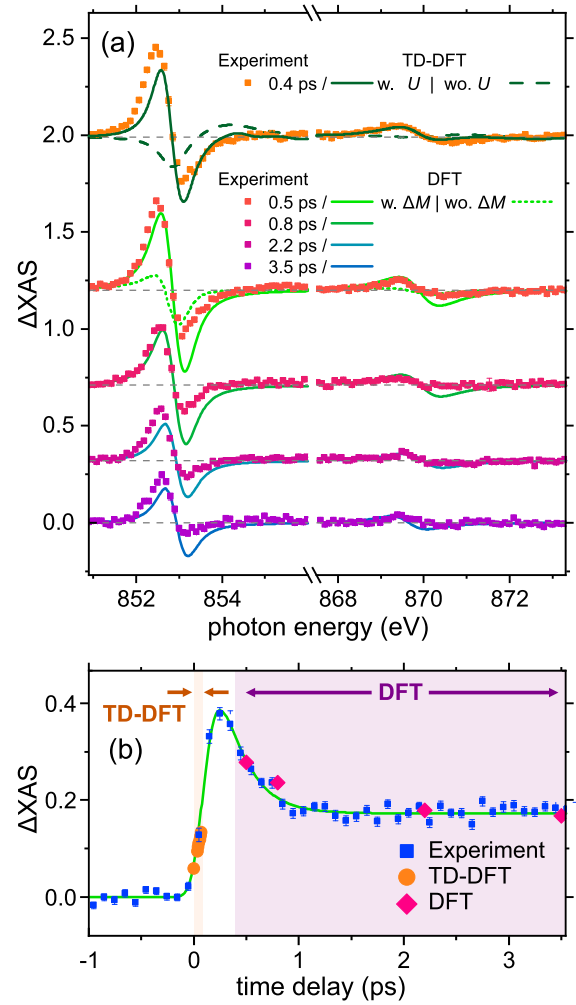
pump-induced change is calculated as the negative logarithm of the pumped signal divided by the unpumped one in combination with flat-field and non-linearity corrections [28]. The spectra are corrected with a linear background and are normalized according to the edge jump [18].

Figure 1(b) depicts the ground state (unpumped) and pumped fcc Ni  $L_3$  edge spectra at  $\Delta t = 0.4$  ps, Figure 1(c) the pump-induced change of the absorption spectrum. A positive change is observed at the rising edge around 852.0–852.8 eV, followed by a smaller negative change at 853–854 eV. To model these changes, we need to account for both a spectral redshift and a broadening by modifying the unpumped spectrum, respectively, with a rigid redshift and a broadening via convolution, fitted to the measured  $\Delta XAS$  [18]. We quantify the redshift to  $104 \pm 25$  meV and the broadening to  $139 \pm 10$  meV, which we assign in the following to changes in the electronic structure respectively electron redistribution. The latter can be intuitively understood from the excitation of holes (electrons) below (above)  $E_F$  by the pump pulse [29], see Figure 1(a).

Figure 2(a) details the spectral dependence of the pump-induced change for  $0.4 \text{ ps} \leq \Delta t \leq 3.5 \text{ ps}$  at both absorption edges. We find that the positive change at lower photon energy recedes to about half within 3.5 ps while keeping its overall shape. The  $L_2$  edge generally exhibits a smaller and energetically broader change, which we explain by the larger lifetime broadening at the  $L_2$  compared to the  $L_3$  edge [18].

We now look at the time dependence in more detail by scanning  $\Delta t$ . Figure 2(b) shows the evolution of the absorption change at a constant  $h\nu = 852.72$  eV, confirming the change at fixed  $h\nu$  reported in Figure 2(a). These time-dependent data highlight that the large change occurs within 200 fs after pumping, while the excess energy resides mostly in the electronic system. The experimental data were fitted with exponential rise and decay times  $\tau_{1,2}$ , respectively, convoluted with a Gaussian of 80 fs FWHM to account for the time resolution [18]. We find  $\tau_1 = 130 \pm 26$  fs and  $\tau_2 = 233 \pm 11$  fs, which we assign to electron thermalization and electron-phonon coupling in good agreement with previous work [30,31].

For a theoretical analysis of the optically induced non-equilibrium state we employ TDDFT, which extends the ground state DFT to the time domain through the exact one-to-one correspondence between the time-dependent external potential and the density [32]. The time-dependent Hamiltonian of an interacting system is mapped onto an equivalent non-interacting one known as the time-dependent Kohn-Sham (TDKS) Hamiltonian with an effective Kohn-Sham (KS) external potential that produces the same density of the interacting system [18].



**Figure 2.** (a) Pump-induced changes  $\Delta XAS$  at the indicated time delays from the experiment (markers) and TDDFT, respectively, DFT calculations (solid lines). For comparison, TDDFT calculations without local correlations (dashed line) and DFT calculations without (dotted line) a reduced magnetization (see text for details), are shown. Traces are vertically offset for easier viewing. (b) Time-dependent  $\Delta XAS$  at  $h\nu = 852.72$  eV with a fit (green line) and the corresponding values from TDDFT (convoluted with a Gaussian of 80 fs FWHM) and DFT, as indicated.

This allows to simulate the dynamics of matter subject to a time-dependent perturbation, e.g. the effect of an optical pulse on the electronic structure [33,34]. A general approach for calculating time-dependent XAS using a mixed scheme between the linear response of TDDFT and the time evolution of the TDKS is outlined in Ref. [35] and the static response function  $\chi_0$  of the KS quasiparticles is given by

$$\chi_0(\omega) = \lim_{\eta \rightarrow 0} \sum_{ijk} (f_{ik} - f_{jk}) \frac{\phi_{ik}^*(\mathbf{r}) \phi_{jk}^*(\mathbf{r}') \phi_{ik}(\mathbf{r}') \phi_{jk}(\mathbf{r})}{\omega - (\epsilon_i - \epsilon_j) + i\eta}. \quad (1)$$

Here  $f_{ik}$  is the occupation of the KS state,  $\phi$  is the single particle KS state,  $i, j$  are band indices,  $k$  is the electron's crystal momentum,  $\eta$  is proportional to lifetime broadening, and  $\epsilon_i$  is the KS energy [36]. This approach has previously been used to provide a qualitative description of time-resolved  $x$ -ray magnetic circular dichroism spectra using only the transient KS populations [35,37]. Here, we use the full transient quantities in Equation (1), namely occupations, energies, and KS orbitals projected on the ground state, following [38]. We introduce the electronic correlations to our system from the single-band Hubbard model and consider a Hamiltonian of the form

$$\hat{H} = \hat{H}_0(t) + U \sum_i n_{i\uparrow}(t)n_{i\downarrow}(t), \quad (2)$$

where  $\hat{H}_0$  is the quasiparticle Hamiltonian assumed to be equivalent to the KS Hamiltonian in the Local Spin Density Approximation (LSDA),  $U$  is the onsite Hubbard correlation, and  $n_{\uparrow,\downarrow}$  are the number operators of spin up and spin down electrons for site  $i$ , respectively. The magnetic response function corresponding to  $\hat{H}$  in mean field (in the Random Phase Approximation) solution is

$$\chi_0^H(\omega) = \lim_{\eta \rightarrow 0} \sum_{ijk} (f_{ik} - f_{jk}) \frac{\phi_{ik}^*(\mathbf{r})\phi_{jk}^*(\mathbf{r}')\phi_{ik}(\mathbf{r}')\phi_{jk}(\mathbf{r})}{\omega - (\epsilon_i - \epsilon_j + U \cdot m) + i\eta}, \quad (3)$$

where  $m = \langle n_{\uparrow} \rangle - \langle n_{\downarrow} \rangle$  is the average magnetization. Equation (3) implies that those optical excitations of an initial ground state ( $\epsilon_i - \epsilon_j$ ) that are accompanied by spin flips experience a shift of  $U \cdot m$  [38].

Before electron thermalization through electron-electron scattering on few 100 fs timescales [29,39], the transient change in the populated DOS is considered as the product of a time- and energy-dependent non-equilibrium distribution function  $f(E, t)$  and an equally time- and energy-dependent DOS( $E, t$ ). Figure 3(a) shows the calculated  $f \cdot \text{DOS}$  for fcc Ni before the optical excitation (unpumped) and after pumping with the experimental pulse parameters at  $\Delta t = 74$  fs, the longest computationally possible propagation time. Upon excitation we find an increase in  $3d_{\downarrow}$  orbitals within an interval of  $\pm 0.2$  eV around  $E_F$ . This behavior is explained by spin-orbit coupling mediated spin currents in the optically excited electron system that induce spin-flip transitions from the majority to the minority channel and lead to a reduced value of  $m$  [9,10]. At 100 fs  $m$  is reduced by  $\approx 15\%$  from the equilibrium value of  $0.61 \mu_B$ . The transient populations and energies are used as input for calculations of absorption spectra at the Ni  $L_{2,3}$  edges following Equation (1) and the results are depicted in Figure 3(b), left. The excited electron distribution leads to a reduction of the absorption peak's height, which captures part

of the experimental XAS in Figure 1(b). The calculated absorption spectra using the time evolution of the TDKS equation within the adiabatic LSDA, presented in Figure 3(b) on the left, are thus well in line with the calculated  $f \cdot \text{DOS}$  in Figure 3(a), but they lack the spectral shift observed in the experiment, see Figure 1(b). While this approximation successfully captures the changes in the occupations  $f_{ik} - f_{jk}$ , it is deficient in reproducing the changes in the excitation energies, signaling the influence of electron correlations. To account for these we adopt Equation (2), using  $U = 3$  eV for the on-site correlation [40]. The correlations modify the excitation energies of the non-interacting KS response function of Equation (1) by the  $U \cdot m$  term, see Equation (3). Calculations of the absorption spectrum including  $U$  are depicted in Figure 3(b) at right and now indeed show the transient redshift. Since the reduced  $m$  is already obtained in the calculations without  $U$ , the ultrafast redshift is assigned to the cooperation of  $U$  and  $m$ , leading to changes in the DOS. We stress that such modifications of the electronic structure are essential to describe the experimental data, as will be shown in the following.

In the top part of Figure 2(a), we compare  $\Delta\text{XAS}$  calculated by TDDFT at  $\Delta t = 0.1$  ps [18] with the earliest full spectrum available at  $\Delta t = 0.4$  ps quantitatively and obtain a very good agreement between experiment and theory. For comparison, we calculate the spectral changes for  $U=0$  and find them to be qualitatively different, see Figure 2(a), and thus unable to describe the experimental observation. In Figure 2(b), the calculated changes from TDDFT and DFT are shown on top of the time-dependent measurement at fixed  $h\nu$ . TDDFT covers  $\Delta t < 100$  fs of the initial absorption increase, reinforcing that the initial non-equilibrium state involves correlation-induced modifications of the electronic structure. In contrast, the spectral shift causing the transient absorption increase at this energy is entirely absent for  $U=0$ , see Figure 3(b). The influence of electron correlations on Ni spin dynamics was also theoretically predicted in [41], justifying our approach.

Previous work [37,42] used transient electronic occupations of ground state wavefunctions to calculate the response function. However, this implies a mere redistribution of occupation weights on a rigid ground state band structure. In similar state blocking calculations [43] some transient features emerge below and above the X-ray absorption edge, but they miss the experimentally observed spectral shift of the entire edge. We instead use the full transient quantities, i.e. we expand the wavefunctions in occupations and energies of instantaneous eigenstates to the transient Hamiltonian to calculate the response function, allowing us to follow the real-time



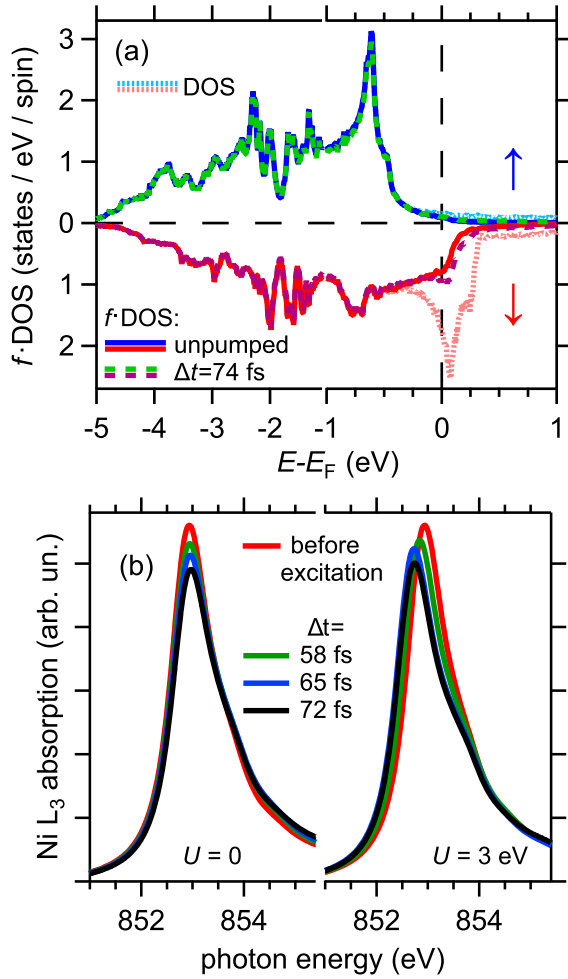


**Figure 3.** (a) Calculated populated exchange-split density of states for KS states in fcc Ni:  $f \cdot \text{DOS}$  for majority ( $\uparrow$ ) and minority ( $\downarrow$ ) states before optical excitation (solid lines) and at the longest TDDFT propagation time  $\Delta t = 74$  fs (dashed lines). The static DOS without population is shown for comparison (dotted lines). (b) Absorption spectrum of the Ni  $L_3$  edge after optical excitation calculated by TDDFT using the transient  $f \cdot \text{DOS}$  from panel (a) at left and including  $U = 3$  eV following Equations (2), (3) in addition to  $f \cdot \text{DOS}$  at right.

dynamics of the response function in agreement with our high-resolution time-resolved XAS experiment.

At times too long for TDDFT to be carried out accurately, we approximate the excited state by an elevated electron temperature  $T_e$  and a reduced  $m$  [8] in quasi-static constrained DFT calculations. In Figure 2(a), the measured  $\Delta\text{XAS}$  is compared with these DFT results for  $\Delta t \geq 0.5$  ps. We find very good agreement for  $T_e$  relaxing from 570 K to 340 K, combined with reduced magnetic moments per atom of  $\mu = 0.47 \mu_B$  to  $0.56 \mu_B$ , for  $0.5 \text{ ps} < \Delta t < 3.5 \text{ ps}$ . Taking only an increased  $T_e$  into account and keeping  $m$  constant is insufficient to obtain the observed  $\Delta\text{XAS}$ , which highlights the sensitivity of this technique to the changed  $m$  even using

linearly polarized  $x$ -rays. We note that earlier work using DFT [43] obtained a spectral redshift for extreme  $T_e$  of 7000 K without considering either  $U$  or the transient spin currents, which determine the ultrafast demagnetization. For more realistic  $T_e$  used here, such an approach can only capture the spectral changes partially. Agreement with our DFT calculations is also found in Figure 2(b) after electron thermalization at  $\Delta t > 400$  fs and for the subsequent cooling of  $T_e$  and simultaneous relaxation of the optically induced demagnetization.

Based on the good agreement of both theory sets with experiment, within their complementary time intervals, we assign the transient spectral broadening to electronic redistribution described by  $f(E, t)$ . The experimentally observed spectral broadening of  $130 \pm 10$  meV indeed agrees reasonably well with  $T_e = 570$  K at 0.5 ps (i.e.  $\Delta T_e = 270$  K above room temperature) considering that  $4 \cdot k_B \Delta T_e = 93$  meV. Deviations between experiment and theory in the negative change of  $\Delta\text{XAS}$ , which get more pronounced with  $\Delta t$  (compare Figure 2(a)), are potentially due to effects not covered in theory, e.g. (non-thermal) phonon transport into the substrate which occurs on these few-ps timescales [44,45].

In conclusion, we present experimental tr-XAS for fcc Ni in the non-equilibrium regime after fs laser excitation in combination with *ab initio* theory, which allows to identify the optically induced electron repopulation and demagnetization. Our combined time and energy resolution further explains the transient redshift of the absorption spectrum as a signature of electron correlations, as signaled by the Hubbard  $U$  and its influence on the electronic response function. This successful demonstration of our theory on a mean field, Hartree-Fock level potentially offers a more general understanding of the influence of local correlations on non-equilibrium charge carrier dynamics not only in similar systems, e.g. Fe and Co [2], but also strongly correlated materials with emergent phases [46]. We note that the theoretical analysis presented here does not rely on a renormalized screening of the Hubbard  $U$  and is in this sense consistent with recent work on NiO [47]. Our approach of combining state-of-the-art time and energy resolution in soft  $x$ -ray absorption spectroscopy with *ab initio* theory thus paves the way for full access to the non-equilibrium electronic structure and many-body effects of the broad class of solid materials that exhibit local correlations and magnetic order.

## Acknowledgments

The authors acknowledge European XFEL in Schenefeld, Germany, for provision of X-ray free-electron laser beamtime at the SCS instrument and would like to thank the staff for their assistance.

## Notes on contributor

**T. L.** performed the experiments and analyzed the data. **M. E.** developed the extension of TDDFT and did the calculations. Both contributed equally to this work.

## Disclosure statement

No potential conflict of interest was reported by the author(s).

## Funding

Funding by the Deutsche Forschungsgemeinschaft (DFG, German Research Foundation) – Project-ID 278162697 – SFB 1242 is gratefully acknowledged. The computations were enabled by resources provided by the Swedish National Infrastructure for Computing (SNIC) at NSC and Uppmax partially funded by the Swedish Research Council through grant agreement no. 2018-05973. O. G. acknowledges financial support from the Strategic Research Council (SSF) grant ICA16-0037 and the Swedish Research Council (VR) grant 2019-03901. This work was also supported by the European Research Council via Synergy Grant 854843 - FASTCORR. O. E. acknowledges support also from eSENCE, the Knut and Alice Wallenberg foundation, the Swedish Research Council (VR) and the Foundation for Strategic Research. C.B. was supported by the Region Grand Est [grant number 19P07304 - FEMTOSPIN]. P. S. M., R. Y. E. and M. B. acknowledge funding from the Helmholtz Association [grant number VH-NG-1105]. We acknowledge support by the Open Access Publication Fund of the University of Duisburg-Essen.

## References

- [1] Suhl H. Magnetism. Vol. 5. New York and London: Elsevier; 1973.
- [2] Sanchez-Barriga J, Braun J, Minar J, et al. Effects of spin-dependent quasiparticle renormalization in Fe, Co, and Ni photoemission spectra. *Phys Rev B*. 2012;85:Article ID 205109. DOI:10.1103/PhysRevB.85.205109
- [3] Stöhr J, Siegmann HC. Magnetism. Vol. 5, Berlin, Heidelberg: Springer; 2006. (Solid-state sciences; 236).
- [4] Schaefer J, Schrupp D, Rotenberg E, et al. Electronic quasiparticle renormalization on the spin wave energy scale. *Phys Rev Lett*. 2004 Mar;92:Article ID 097205. DOI:10.1103/PhysRevLett.92.097205
- [5] Kittel C, Abrahams E. Relaxation process in ferromagnetism. *Rev Mod Phys*. 1953;25(1):233–238
- [6] Beaupaire E, Merle JC, Daunois A, et al. Ultrafast spin dynamics in ferromagnetic nickel. *Phys Rev Lett*. 1996 May;76:4250–4253.
- [7] Kirilyuk A, Kimel AV, Rasing T. Ultrafast optical manipulation of magnetic order. *Rev Mod Phys*. 2010;82(3):2731–2784.
- [8] Koopmans B, Malinowski G, Dalla Longa F, et al. Explaining the paradoxical diversity of ultrafast laser-induced demagnetization. *Nat Mater*. 2015;9:Article ID 217204.
- [9] Töws W, Pastor GM. Many-body theory of ultrafast demagnetization and angular momentum transfer in ferromagnetic transition metals. *Phys Rev Lett*. 2015 Nov;115:Article ID 217204. DOI:10.1103/PhysRevLett.115.217204
- [10] Krieger K, Dewhurst JK, Elliott P, et al. Laser-induced demagnetization at ultrashort time scales: predictions of tddft. *J Chem Theory Comput*. 2015;11(10):4870–4874. DOI:10.1021/acs.jctc.5b00621
- [11] Battiato M, Carva K, Oppeneer PM. Theory of laser-induced ultrafast superdiffusive spin transport in layered heterostructures. *Phys Rev B*. 2012 Jul;86:Article ID 024404. DOI:10.1103/PhysRevB.86.024404
- [12] Dewhurst JK, Elliott P, Shallcross S, et al. Laser-induced intersite spin transfer. *Nano Lett*. 2018 Mar;18(3):1842–1848. DOI:10.1021/acs.nanolett.7b05118
- [13] Hofherr M, Häuser S, Dewhurst JK, et al. Ultrafast optically induced spin transfer in ferromagnetic alloys. *Sci Adv*. 2020;6(3):eaay8717. DOI:10.1126/sciadv.aay8717
- [14] Dornes C, Acremann Y, Savoini M, et al. The ultrafast einstein–de haas effect. *Nature*. 2019;565(7738):209–212.
- [15] Tauchert SR, Volkov M, Ehberger D, et al. Polarized phonons carry angular momentum in ultrafast demagnetization. *Nature*. 2022;602(7895):73–77.
- [16] Tschentscher T, Bressler C, Gruenert J, et al. Photon beam transport and scientific instruments at the European XFEL. *Appl Sci*. 2017;7(6):592.
- [17] Decking W, Abeghyan S, Abramian P, et al. A MHz-repetition-rate hard x-ray free-electron laser driven by a superconducting linear accelerator. *Nat Photon*. 2020;14:391–397.
- [18] See the supplement for more information on the sample preparation and theoretical method as well as the analysis and fitting of the measured spectra.
- [19] Gerasimova N, La Civita D, Samoylova L, et al. *J Synchrotron Rad*. 2022;29:1299–1308.
- [20] Data recorded for the experiment at the European XFEL are available at DOI:10.22003/XFEL.EU-DATA-002161-00
- [21] Pergament M, Palmer G, Kellert M, et al. Versatile optical laser system for experiments at the european x-ray free-electron laser facility. *Opt Express*. 2016;24(26):Article ID 29349.
- [22] Döring F, Rösner B, Langer M, et al. Multifocus off-axis zone plates for x-ray free-electron laser experiments. *Optica*. 2020;7(8):1007.
- [23] Le Guyader L, Eschenlohr A, Beye M, et al. Photon-shot-noise-limited transient absorption soft X-ray spectroscopy at the European XFEL. *J Synchrotron Radiat*. 2023 Mar;30(2):284–300. DOI:10.1107/S1600577523000619.
- [24] Porro M, Andricek L, Aschauer S, et al. The minisdd-based 1-mpixel camera of the dssc project for the european xfel. *IEEE Trans Nucl Sci*. 2021;68(6):1334–1350.
- [25] Fangohr H, Beg M, Bondar V, et al. Data analysis support in karabo at European XFEL. In: Proc. of international conference on accelerator and large experimental control systems (ICALEPCS'17). Geneva, Switzerland: JACoW; 2018 Jan p. 245–252. (International conference on accelerator and large experimental control systems; 16). DOI:10.18429/JACoW-ICALEPCS2017-TUCPA01
- [26] Castoldi A, Porro M, Turcato M, et al. Calibration strategy of the dssc x-ray imager. In: 2019 IEEE Nuclear Science Symposium and Medical Imaging Conference (NSS/MIC); 2019. p. 1–3.
- [27] Fangohr H, Beg M, Bergemann M, et al. Data exploration and analysis with jupyter notebooks. In: Proc. ICALEPCS'19; 08. Geneva: JACoW Publishing; 2020. p. 799–806. (International conference on accelerator

- and large experimental physics control systems; 17). DOI:10.18429/JACoW-ICALEPCS2019-TUCPR02.
- [28] LeGuyader L. SCS toolbox. 2022. Available from: [git.xfel.eu/SCS/ToolBox](https://git.xfel.eu/SCS/ToolBox).
- [29] Rhie HS, Dürr HA, Eberhardt W. Femtosecond electron and spin dynamics in ni/w(110) films. *Phys Rev Lett.* 2003 Jun;90(24):Article ID 247201. DOI:10.1103/PhysRevLett.90.247201
- [30] Stamm C, Kachel T, Pontius N, et al. Femtosecond modification of electron localization and transfer of angular momentum in nickel. *Nat Mater.* 2007 Oct;6(10):740–743. Available from: <http://www.nature.com/articles/nmat1985>.
- [31] Stamm C, Pontius N, Kachel T, et al. Femtosecond x-ray absorption spectroscopy of spin and orbital angular momentum in photoexcited ni films during ultrafast demagnetization. *Phys Rev B.* 2010 Mar;81:Article ID 104425. DOI:10.1103/PhysRevB.81.104425
- [32] Runge E, Gross EKV. Density-functional theory for time-dependent systems. *Phys Rev Lett.* 1984 Mar;52:997–1000. DOI:10.1103/PhysRevLett.52.997
- [33] Castro A, Marques MAL, Alonso JA, et al. Optical properties of nanostructures from time-dependent density functional theory. *J Comput Theor Nanosci.* 2004 Oct;1(3):231–255. DOI:10.1166/jctn.2004.2931
- [34] Bertsch GF, Iwata JI, Rubio A, et al. Real-space, real-time method for the dielectric function. *Phys Rev B.* 2000 Sep;62:7998–8002. DOI:10.1103/PhysRevB.62.7998
- [35] Dewhurst J, Willems F, Elliott P, et al. Element specificity of transient extreme ultraviolet magnetic dichroism. *Phys Rev Lett.* 2020 Feb;124(7):Article ID 077203. DOI:10.1103/PhysRevLett.124.077203
- [36] Petersilka M, Gossmann UJ, Gross EKV. Excitation energies from time-dependent density-functional theory. *Phys Rev Lett.* 1996 Feb;76(8):1212–1215. DOI:10.1103/PhysRevLett.76.1212
- [37] Yao K, Willems F, von Korff Schmising C, et al. Distinct spectral response in M-edge magnetic circular dichroism. *Phys Rev B.* 2020 Sep;102(10):Article ID 100405. DOI:10.1103/PhysRevB.102.100405
- [38] Elhanoty MF, Grånäs O, Eriksson O, et al. 2023.to be published
- [39] Chang HT, Guggenmos A, Cushing SK, et al. Electron thermalization and relaxation in laser-heated nickel by few-femtosecond core-level transient absorption spectroscopy. *Phys Rev B.* 2021 Feb;103(6):Article ID 064305. DOI:10.1103/PhysRevB.103.064305
- [40] Bandyopadhyay T, Sarma DD. Calculation of coulomb interaction strengths for 3d transition metals and actinides. *Phys Rev B.* 1989 Feb;39(6):3517–3521. DOI:10.1103/PhysRevB.39.3517
- [41] Acharya SR, Turkowski V, Zhang G, et al. Ultrafast electron correlations and memory effects at work: femtosecond demagnetization in Ni. *Phys Rev Lett.* 2020 Jun;125(1):Article ID 017202. DOI:10.1103/PhysRevLett.125.017202
- [42] Shallcross S, Schmising CK, Elliott P, et al. Electronic origin of x-ray absorption peak shifts. *Phys Rev B.* 2022 Aug;106:Article ID L060302. DOI:10.1103/PhysRevB.106.L060302
- [43] Carva K, Legut D, Oppeneer PM. Influence of laser-excited electron distributions on the x-ray magnetic circular dichroism spectra: implications for femtosecond demagnetization in Ni. *EPL.* 2009;86:Article ID 57002.
- [44] Rothenbach N, Gruner ME, Ollefs K, et al. Microscopic nonequilibrium energy transfer dynamics in a photoexcited metal/insulator heterostructure. *Phys Rev B.* 2019 Nov;100:Article ID 174301. DOI:10.1103/PhysRevB.100.174301
- [45] Rothenbach N, Gruner ME, Ollefs K, et al. Effect of lattice excitations on transient near-edge x-ray absorption spectroscopy. *Phys Rev B.* 2021 Oct;104:Article ID 144302. DOI:10.1103/PhysRevB.104.144302
- [46] Baykusheva DR, Jang H, Husain AA, et al. Ultrafast renormalization of the on-site coulomb repulsion in a cuprate superconductor. *Phys Rev X.* 2022 Jan;12:Article ID 011013. DOI:10.1103/PhysRevX.12.011013
- [47] Grånäs O, Vaskivskyi I, Wang X, et al. Ultrafast modification of the electronic structure of a correlated insulator. *Phys Rev Res.* 2022 Aug;4:Article ID L032030. DOI:10.1103/PhysRevResearch.4.L032030